International Journal of Pharmaceutical research and Applications
Volume 11, Issue 5, Sep.-Oct.2026,pp:1111-1128 www.ijprajournal.com ISSN:2456-4494

Integrated In Silico and In Vitro Evaluation of Flavonoids as Cyclooxygenase-2 Inhibitors and Anti-inflammatory Agents

Ms. Diksha Rahangdale[1], Dr. Rohit Sahu[2], Mr. Anand Prajapati[3]
Shri Rawatpura Sarkar Institute of Pharmacy, Jabalpur, India

Date of Submission: 12-10-2026 Date of Acceptance: 24-10-2026

Abstract
Selective inhibition of cyclooxygenase-2 (COX-2) remains a validated anti-inflammatory strategy, but the cardiovascular liabilities associated with near-complete isoform selectivity have renewed interest in multi-target natural scaffolds with a graded preference for COX-2. We evaluated fourteen structurally diverse flavonoids, with celecoxib as reference, in a workflow in which molecular docking, ADMET prediction, 100 ns molecular dynamics (MD) simulations and matched COX-2/COX-1 enzyme assays complement one another. Docking against human COX-2 (PDB 3LN1; redocking RMSD 0.94 Å) placed all flavonoids in the cyclooxygenase channel (−8.0 to −10.1 kcal/mol) in a conserved mode anchored by Arg120, Tyr355 and Ser530. Quercetin, luteolin and baicalein showed the most favourable drug-likeness, whereas EGCG and rutin were limited by polarity and efflux. In 100 ns GROMACS simulations, the celecoxib, EGCG and quercetin complexes reached stable Cα RMSD plateaus of about 0.22–0.24 nm without drift; the celecoxib complex was the most compact and least mobile, and the flavonoid complexes showed slightly higher fluctuations and solvent exposure. EGCG sustained two to three protein–ligand hydrogen bonds against zero to one for celecoxib, consistent with a hydroxyl-driven binding mode for the flavonoids and a shape-driven mode for the coxib. Fluorometric assays gave COX-2 IC50 values of 1.42–12.35 µM for the flavonoids (celecoxib 0.08 µM) and selectivity indices of 3.1–8.7, in line with the absence of side-pocket occupancy. Docking score tracked pIC50 across the 15 compounds (R^2 = 0.92) and within the flavonoid series (R^2 = 0.97). Structure–activity analysis identified C-ring planarity and a B-ring catechol as the principal potency determinants and 3-O-glycosylation as detrimental. Quercetin and luteolin combine low-micromolar potency, moderate COX-2 preference and favourable drug-likeness, and are proposed as scaffolds for sulfonyl- and ester-based optimisation.

Keywords: *flavonoids; cyclooxygenase-2; molecular docking; molecular dynamics; ADMET; anti-inflammatory*

I. Introduction

Inflammation is the coordinated response through which vascularised tissue recognises injury, contains it and restores homeostasis [1]. In its acute form the response is protective and self-limiting: vasodilatation, increased vascular permeability and the ordered recruitment of neutrophils and monocytes are followed by active termination through specialised pro-resolving mediators [2]. When resolution fails, persistent stimulation by microbial products, autoantigens, crystalline deposits or metabolic stress converts this protective programme into a chronic, tissue-destructive one [3]. Unresolved low-grade inflammation is now recognised as a shared mechanistic thread running through rheumatoid arthritis, osteoarthritis, inflammatory bowel disease, atherosclerosis, type 2 diabetes, neurodegeneration and several malignancies [3,4], and the demand for effective, well-tolerated anti-inflammatory therapy continues to grow.

At the molecular level, the response is governed by an interlocking network of transcriptional and enzymatic events. Pattern-recognition receptors activate nuclear factor-κB (NF-κB) and mitogen-activated protein kinase cascades, which drive expression of tumour necrosis factor-α (TNF-α), interleukin-1β (IL-1β), interleukin-6 (IL-6), inducible nitric oxide synthase (iNOS) and COX-2 [5,6]. TNF-α and IL-1β act as apical cytokines that amplify the response and induce secondary mediators including IL-6 [7,8], whereas iNOS-derived nitric oxide and its reaction products sustain oxidative and nitrosative stress, which in turn re-activates NF-κB [9]. Arachidonic acid released from membrane phospholipids is processed along cyclooxygenase, lipoxygenase and cytochrome P450 routes [10]. Among these effectors, COX-2 occupies a particularly tractable position: it is the rate-limiting enzyme for

International Journal of Pharmaceutical research and Applications
Volume 11, Issue 5, Sep.-Oct.2026,pp:1111-1128 www.ijprajournal.com ISSN:2456-4494

prostanoid biosynthesis at inflamed sites, it is inducible rather than constitutive, and it is the dominant source of prostaglandin E2 in inflamed tissue [11].

Mechanistic clarity in this field arrived in 1971, when Vane showed that aspirin-like drugs suppress prostaglandin synthesis [12]. Cyclooxygenase (prostaglandin-endoperoxide synthase) catalyses the bis-dioxygenation of arachidonic acid to PGG2 and its peroxidase-mediated reduction to PGH2, and exists as two principal isoforms [13]. COX-1 is expressed constitutively in gastric mucosa, kidney and platelets, where its products maintain mucosal integrity, renal perfusion and haemostasis; COX-2 is largely absent from resting tissue and is rapidly induced by cytokines, endotoxin and growth factors [13]. Crystal structures of COX-1 [14] and COX-2 [15] revealed near-identical catalytic machinery (about 60 % sequence identity) but one decisive difference: replacement of isoleucine in COX-1 by valine at position 523 opens a hydrophobic side pocket bounded by Arg513, Phe518, Val523 and His90, which is the structural basis of isoform-selective inhibition [15–17]. The cyclooxygenase site itself is a long hydrophobic channel lined by Arg120, Tyr355, Tyr385, Trp387 and Ser530; Arg120 and Tyr355 form a constriction at the channel mouth that anchors the carboxylate of arachidonic acid and of acidic non-steroidal anti-inflammatory drugs (NSAIDs) [16,17]. Because COX-2 behaves as a conformational heterodimer [16] and side-pocket inhibitors often bind in a slow, time-dependent manner [18], enzyme-level potencies and computed binding energies need to be compared with some care.

Traditional NSAIDs inhibit both isoforms. Their benefit derives from COX-2 blockade, whereas concurrent COX-1 inhibition suppresses cytoprotective gastric prostaglandins and platelet thromboxane, producing the gastroduodenal ulceration and bleeding that dominate NSAID-related hospitalisation [19]. Selective COX-2 inhibitors (coxibs) were developed around the side pocket to separate efficacy from this toxicity and did reduce upper gastrointestinal events [20]. Subsequent cardiovascular safety signals, attributed in large part to suppression of endothelial prostacyclin without a matching reduction in platelet thromboxane [21], led to the withdrawal of rofecoxib [22] and to class-wide warnings. This prothrombotic imbalance scales with the degree of selectivity and with cumulative exposure, so that current thinking favours agents with moderate rather than absolute COX-2 preference, or agents whose additional mechanisms lower the degree of COX-2 blockade required for benefit [20,21].

Flavonoids are well placed to meet this profile. They are plant secondary metabolites built on a C6–C3–C6 diphenylpropane skeleton in which two aromatic rings (A and B) are joined by a three-carbon bridge, usually closed into a heterocyclic C ring; more than ten thousand structures are known [23–25]. Flavones, flavonols, flavanones, flavan-3-ols, isoflavones and anthocyanidins are the principal dietary subclasses [26], and four structural features govern their behaviour: a catechol arrangement on the B ring, a C2–C3 double bond conjugated with the C4 carbonyl, a C3 hydroxyl, and 5,7-hydroxylation of the A ring [24,27]. Pharmacologically, flavonoids are polypharmacological: they inhibit NF-κB activation, scavenge reactive oxygen and nitrogen species, suppress cytokine release from activated macrophages and modulate eicosanoid-forming enzymes [28–31]. Compound-specific reviews document these actions for quercetin [32], luteolin [33], baicalein [34], apigenin [35] and epigallocatechin-3-gallate (EGCG) [36], and structure–activity analyses of cellular mechanisms are available [37].

Direct inhibition of cyclooxygenase by flavonoids has been reported repeatedly in cell-free and cellular systems [38–42]. Flavonols and flavones typically inhibit the enzymes at low-micromolar concentrations, one to two orders of magnitude weaker than celecoxib and with modest isoform preference [38,42]. This pattern is consistent with the structure of the target. The planar chromone nucleus, the aromatic B ring and the pattern of phenolic hydroxyls provide the hydrophobic surface and directional hydrogen-bonding capacity that the main COX channel accommodates, whereas the compact, polar scaffold is unlikely to reproduce the side-pocket occupancy of a coxib sulfonamide; graded rather than absolute selectivity would therefore be expected. Cell-based readouts such as prostaglandin E2 production or COX-2 transcription [39,40] integrate effects on signalling and oxidative stress, so a cell-free enzyme assay is needed to isolate the direct contribution of enzyme binding.

Two limitations temper this promise. First, most dietary flavonoids are polyphenolic and often glycosylated, which restricts passive permeability; extensive conjugation and microbial metabolism

International Journal of Pharmaceutical research and Applications
Volume 11, Issue 5, Sep.-Oct.2026,pp:1111-1128 www.ijprajournal.com ISSN:2456-4494

then make systemic exposure modest and variable [26,43,44], and catechins in particular undergo substantial presystemic extraction [45]. Formulation strategies such as phospholipid complexes and nanocarriers are being developed to address this [46,47]. Second, polyphenols can behave as assay-interference compounds in poorly controlled screens, producing apparent activity that does not survive orthogonal confirmation. Both concerns argue for computational triage that includes absorption, distribution, metabolism, excretion and toxicity (ADMET) prediction, followed by enzyme-level confirmation under defined conditions.

Structure-based computational methods now provide a practical route to such triage. Molecular docking predicts the preferred orientation of a ligand in a binding site and estimates its interaction energy [48], but its rigid or semi-rigid treatment of the receptor and approximate scoring functions mean that it separates plausible from implausible binders better than it ranks close analogues. Molecular dynamics (MD) simulation restores receptor flexibility and explicit solvent, allowing poses to relax and genuinely unstable ones to dissociate, and end-point methods such as MM-PBSA convert the resulting ensemble into binding free energies with per-residue decomposition [49,50]. Drug-likeness and ADMET filters [51,52] evaluated alongside affinity prevent effort from being invested in potent compounds that could never reach the target in vivo. Despite these tools, published studies typically report either computational or experimental endpoints, so that predicted rankings are rarely tested against potencies measured on the same compounds under uniform conditions; simulations are often too short for confident end-point energetics; and isoform selectivity is frequently inferred from COX-2 docking alone, without the matched COX-1 measurement needed to quantify it.

We therefore carried a single set of fourteen flavonoids, plus celecoxib as reference, through a sequence of complementary stages (Figure 1). Docking against the human COX-2 crystal structure proposes a binding mode; 100 ns all-atom MD simulations test whether that mode survives receptor flexibility and explicit solvation; ADMET profiling defines developability; and matched COX-2 and COX-1 inhibition assays supply a quantitative anchor against which each computational stage can be calibrated. The aims were to (i) define the binding mode of the series and its persistence, (ii) measure potency and isoform selectivity under uniform conditions, (iii) test how well the computational stages anticipate experiment, and (iv) derive structure–activity relationships that can guide semi-synthetic optimization.

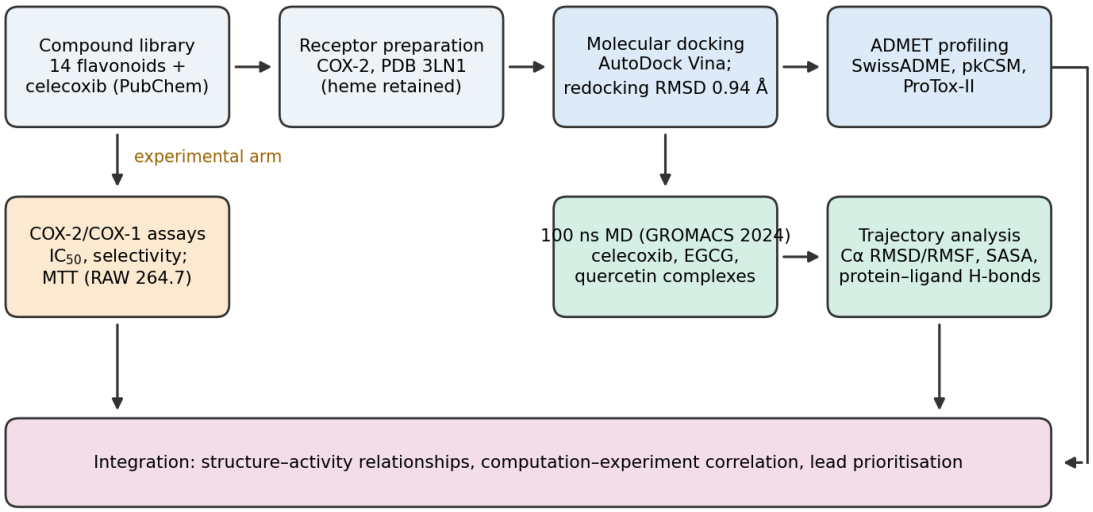

Figure 1. Integrated in silico and in vitro workflow. Each computational stage (blue, green) generates a hypothesis that is tested experimentally (orange), and all outputs converge in a joint analysis of structure–activity relationships and computation–experiment agreement.

International Journal of Pharmaceutical research and Applications
Volume 11, Issue 5, Sep.-Oct.2026,pp:1111-1128 www.ijprajournal.com ISSN:2456-4494

II. Materials and Methods

2.1 Compound library

Fourteen flavonoids were selected to satisfy four criteria: structural coverage, matched pairs, dietary relevance and availability at defined purity. The set comprises four flavonols (quercetin, myricetin, fisetin, kaempferol), four flavones (luteolin, baicalein, apigenin, chrysin), two flavan-3-ols (EGCG, catechin), two flavanones (naringenin, hesperetin), one isoflavone (genistein) and one flavonol glycoside (rutin), so that the influence of C-ring oxidation state, B-ring attachment and glycosylation can be assessed independently. Matched pairs that differ at a single position convert the series from a survey into a structure–activity experiment: luteolin/apigenin and quercetin/kaempferol differ in the 3′-hydroxyl, quercetin/luteolin in the 3-hydroxyl, quercetin/rutin by glycosylation at C3, and naringenin/apigenin in the C2–C3 double bond. Celecoxib was included throughout as the reference selective inhibitor because the question concerns isoform selectivity as well as potency.

Three-dimensional structures were retrieved from PubChem [53] (Table 1), protonated at pH 7.4 and geometry-optimised in Open Babel [54] with the MMFF94 force field (steepest descent, 2000 steps or gradient below 0.01 kcal/mol/Å). Structures were converted to PDBQT format in AutoDockTools [55] with Gasteiger charges and merged non-polar hydrogens, and all acyclic single bonds were left free to rotate.

Table 1. Composition of the compound library.

Compound	Subclass	PubChem CID	Formula	MW (g/mol)
Celecoxib	Reference (coxib)	2662	C17H14F3N3O2S	381.37
EGCG	Flavan-3-ol	65064	C22H18O11	458.37
Quercetin	Flavonol	5280343	C15H10O7	302.24
Luteolin	Flavone	5280445	C15H10O6	286.24
Myricetin	Flavonol	5281672	C15H10O8	318.24
Baicalein	Flavone	5281605	C15H10O5	270.24
Fisetin	Flavonol	5281614	C15H10O6	286.24
Kaempferol	Flavonol	5280863	C15H10O6	286.24
Apigenin	Flavone	5280443	C15H10O5	270.24
Genistein	Isoflavone	5280961	C15H10O5	270.24
Rutin	Flavonol glycoside	5280805	C27H30O16	610.52
Chrysin	Flavone	5281607	C15H10O4	254.24
Naringenin	Flavanone	932	C15H12O5	272.25
Hesperetin	Flavanone	72281	C16H14O6	302.28
Catechin	Flavan-3-ol	9064	C15H14O6	290.27

2.2 Receptor preparation

The crystal structure of human COX-2 in complex with celecoxib (PDB 3LN1, 2.40 Å) [56] was prepared in UCSF Chimera [57]. Chain A was retained; crystallographic waters, the co-crystallised ligand, detergent molecules and N-acetylglucosamine glycosylation units were removed, whereas the catalytically essential protoporphyrin IX heme and its iron were kept. Missing side-chain atoms were rebuilt, histidine protonation states were assigned from the local hydrogen-bonding environment, polar hydrogens were added at pH 7.4 and Kollman united-atom charges were applied. Stereochemical quality was confirmed by Ramachandran analysis, with 95.8 % of residues in favoured regions and no outliers among active-site residues.

2.3 Molecular docking

Docking was carried out with AutoDock Vina [48,58]. The grid (26 × 26 × 26 Å, 1.0 Å spacing) was centred on the co-crystallised celecoxib (x = 25.14, y = 22.68, z = 15.37 Å) and encloses the whole cyclooxygenase channel, from the Arg120/Tyr355 constriction to Ser530, together with the Val523 side pocket, while excluding the spatially separate peroxidase site. The receptor was held rigid and ligands were fully flexible. Exhaustiveness was 24, the energy range 4 kcal/mol, and up to 20 modes were retained per ligand. Each ligand was docked in triplicate with different random seeds and the mean best score is reported; the pose carried forward was the top-ranked member of the most populated cluster (2.0 Å RMSD threshold). The protocol was validated by redocking

International Journal of Pharmaceutical research and Applications
Volume 11, Issue 5, Sep.-Oct.2026,pp:1111-1128 www.ijprajournal.com ISSN:2456-4494

celecoxib under identical settings, with an RMSD below 2.0 Å as the acceptance criterion.

Interactions were analysed in Discovery Studio Visualizer. Hydrogen bonds were assigned by a donor–acceptor distance up to 3.5 Å and a donor–hydrogen–acceptor angle above 120°, π-stacking by a centroid separation below 5.5 Å and an interplanar angle below 30°, and hydrophobic contacts by non-polar heavy-atom separations below 4.5 Å. Contacts were compiled across the thirteen residues lining the channel.

2.4 ADMET prediction

Physicochemical descriptors, drug-likeness (Lipinski [51], Ghose, Veber [52], Egan and Muegge rules), BOILED-Egg passive absorption [59], P-glycoprotein substrate status and cytochrome P450 inhibition were obtained from SwissADME [60]. pkCSM [61] supplied Caco-2 permeability, intestinal absorption, volume of distribution, fraction unbound, blood–brain barrier permeability, CYP classification, total clearance and renal OCT2 status, and ProTox-II [62] supplied predicted median lethal dose, toxicity class and organ-level toxicity endpoints. Canonical SMILES generated from the optimised structures were used as input to all platforms so that results are comparable.

2.5 Molecular dynamics simulations

Three systems were simulated: the celecoxib complex and the complexes of the two top-ranked flavonoids, EGCG and quercetin, each built from the best docked pose. Systems were assembled in CHARMM-GUI Solution Builder [63] and simulated with GROMACS 2024 [64], using the CHARMM36m force field [65] for the protein, CGenFF [66] for the ligands (penalty scores below 10 for all assigned parameters) and TIP3P water [67]. Each complex was placed in a cubic box with at least 1.2 nm between solute and wall, solvated, and neutralised with Na+ and Cl− to 0.15 M. Systems were minimised by steepest descent, equilibrated for 500 ps in the NVT ensemble at 310 K with the V-rescale thermostat [68] under heavy-atom position restraints, and then for 1 ns in the NPT ensemble at 1 bar with the Parrinello–Rahman barostat [69] while the restraints were released stepwise. Production runs of 100 ns followed in the NPT ensemble (Table 2), with LINCS constraints on hydrogen-containing bonds [70] and particle-mesh Ewald electrostatics [71]. Simulations were run on a GPU-accelerated workstation (Ubuntu 22.04, NVIDIA RTX 4050).

Table 2. Molecular dynamics set-up.

Parameter	Specification
Software	GROMACS 2024
Systems	COX-2 complexes with celecoxib, EGCG and quercetin (one trajectory each)
Force fields	CHARMM36m (protein); CGenFF (ligands); TIP3P (water)
Box and ionic strength	Cubic, 1.2 nm padding; 0.15 M NaCl
Minimisation	Steepest descent, up to 50,000 steps, Fmax < 1000 kJ/mol/nm
Equilibration	NVT 500 ps (310 K, V-rescale); NPT 1 ns (1 bar, Parrinello–Rahman)
Production	100 ns per system, NPT, 2 fs time step
Constraints and non-bonded	LINCS on H-bonds; PME with 1.2 nm real-space cut-off; force-switched vdW 1.0–1.2 nm

Trajectories were corrected for periodicity and fitted to the starting structure by least-squares superposition of the protein Cα atoms. Cα RMSD and per-position RMSF were calculated with gmx rms and gmx rmsf, the solvent-accessible surface area (SASA) of the protein with gmx sasa, and protein–ligand hydrogen bonds with gmx hbond (donor–acceptor distance up to 3.5 Å and donor–hydrogen–acceptor angle within 30° of linearity). Equilibration was judged from the plateau behaviour of the RMSD and from the absence of drift over the final 40 ns of each trajectory. Time series were plotted with Grace.

2.6 COX-1 and COX-2 inhibition assays

Quercetin, luteolin, kaempferol, apigenin, myricetin, fisetin, baicalein, genistein, rutin, chrysin, naringenin, hesperetin, catechin, EGCG and celecoxib (≥ 95 % purity by HPLC) were obtained from Sigma-Aldrich and prepared as 20 mM stocks in DMSO (−20 °C, protected from light). Working dilutions were prepared fresh in assay buffer so that

International Journal of Pharmaceutical research and Applications
Volume 11, Issue 5, Sep.-Oct.2026,pp:1111-1128 www.ijprajournal.com ISSN:2456-4494

the final DMSO concentration never exceeded 0.5 % (v/v), a level shown in preliminary experiments to be without effect on enzyme activity. Eight concentrations spanning three orders of magnitude and centred on the potency range found in pilot experiments were used for each compound.

COX activity was measured with a commercial fluorometric inhibitor screening kit (ovine COX-1, human recombinant COX-2, arachidonic acid, ADHP probe, heme) in black 96-well plates. Buffer, heme and enzyme were combined with test compound or vehicle and pre-incubated for 10 min at 25 °C; the reaction was started by simultaneous addition of arachidonic acid and ADHP, and the peroxidase-dependent formation of resorufin was followed kinetically for 5 min (excitation 535 nm, emission 587 nm). Each plate carried a 100 % activity control, a no-enzyme background control and a celecoxib series. Plate layouts were randomised with respect to concentration and normalisation was internal to each plate. Rates were taken from the linear portion of each trace and inhibition was calculated as (rate of control − rate of sample)/rate of control × 100 after background subtraction. Percentage inhibition was fitted against log concentration to a four-parameter logistic model in GraphPad Prism 9.5 with top and bottom constrained to 100 % and 0 %. The selectivity index (SI) was defined as IC50(COX-1)/IC50(COX-2), so that values above 1 indicate preferential COX-2 inhibition. All determinations were performed in triplicate in three independent experiments on separate days with freshly diluted aliquots, so that the reported variability reflects inter-experiment rather than intra-plate scatter.

2.7 Cytotoxicity assay

RAW 264.7 murine macrophages (National Centre for Cell Science, Pune) were maintained in Dulbecco's modified Eagle medium with 10 % fetal bovine serum and 1 % penicillin–streptomycin at 37 °C under 5 % CO2, seeded at 1 × 10^4 cells per well in 96-well plates and, after overnight adhesion, treated with the four lead compounds at 1, 5, 10, 25, 50 and 100 µM for 24 h. Viability was measured by the MTT assay [73] (0.5 mg/mL, 4 h; formazan dissolved in DMSO; absorbance at 570 nm with a 630 nm reference) and expressed relative to vehicle-treated cells.

2.8 Statistical analysis and reproducibility

Data are mean ± SD of three independent experiments (docking: three random seeds). Group comparisons used one-way ANOVA followed by Dunnett's test against vehicle ($p < 0.05$). The relationship between computed and measured quantities was examined by linear regression of pIC50 (−log10 of the IC50 in mol/L) on docking score, reporting Pearson r and R^2, and robustness was tested by leave-one-out analysis. Docking, trajectory analysis and statistics were scripted and kept under version control so that the computational results can be reproduced exactly.

III. Results and Discussion

3.1 Docking validation and binding affinities

Redocking of celecoxib into the prepared receptor reproduced the crystallographic pose with a heavy-atom RMSD of 0.94 Å, well inside the 2.0 Å acceptance criterion, and recovered both the sulfonamide contacts with His90, Gln192 and Arg513 in the side pocket and the contacts of the trifluoromethylpyrazole core with Val349, Leu352 and Ala527. Reproduction of the pose and of its key polar contacts indicates that the grid, receptor model and scoring settings are fit for this compound class.

All 15 compounds docked within the cyclooxygenase channel with affinities between −8.0 and −11.2 kcal/mol (Figure 2a). Celecoxib scored best (−11.2 kcal/mol), 1.1 kcal/mol ahead of the top flavonoid, EGCG (−10.1), which was followed by quercetin (−9.8), luteolin (−9.6), myricetin (−9.5) and baicalein (−9.4); eight flavonoids passed the −9.0 kcal/mol threshold adopted for progression. Standard deviations over triplicate runs did not exceed 0.2 kcal/mol, indicating reproducible convergence. Grouping by subclass (Figure 2b) shows the ordering planar flavonols (mean −9.45 kcal/mol) > flavones (−9.15) > flavan-3-ols (−9.05) > isoflavone (−8.9) > glycoside (−8.7) > flavanones (−8.3).

This ranking follows a clear structural logic. The 3-hydroxylated flavonols combine an extended conjugated, planar chromone with additional hydrogen-bond donors, whereas the puckered C ring of the flavanones displaces the B ring from the chromone plane and reduces complementarity along the channel. The glycoside rutin sits mid-table despite its size, reflecting extensive but less efficient surface contact. The wide spread within the flavan-3-ols, from EGCG at the top to catechin at the bottom, foreshadows the contribution of the galloyl ester. Because empirical scoring functions discriminate plausible from implausible binders better than they rank close analogues [48], the docking scores are treated here

International Journal of Pharmaceutical research and Applications
Volume 11, Issue 5, Sep.-Oct.2026,pp:1111-1128 www.ijprajournal.com ISSN:2456-4494

as a structural hypothesis to be tested by simulation and assay rather than as quantitative affinity predictions.

3.2 A conserved binding architecture without side-pocket occupancy

The flavonoid poses share a common architecture. The chromone nucleus lies along the hydrophobic channel, the A-ring hydroxyls project towards the Arg120/Tyr355 constriction at the channel mouth, and the B ring orients towards Tyr385 and Ser530 at the apex. This arrangement places the catechol hydroxyls within hydrogen-bonding range of the residues most closely tied to catalysis and offers a direct structural rationale for inhibition. Quercetin exemplifies the pattern: its 3′- and 4′-hydroxyls donate hydrogen bonds to Ser530 and Tyr385, the 3-hydroxyl and 4-carbonyl of the C ring engage Tyr355 and Arg120, and the A ring stacks against Trp387 (centroid separation 4.6 Å), while Val349, Leu352, Val523 and Ala527 maintain hydrophobic contact. EGCG reaches its additional affinity by a different route: its galloyl ester extends towards the entrance of the side pocket and hydrogen-bonds Arg513, the chromanol hydroxyls engage Arg120, Tyr355 and Ser530, and six hydrogen bonds are formed in total, the highest count in the series.

Across the library, Arg120 and Tyr355 were engaged by 14 of the 15 compounds, and Val349, Leu352, Val523 and Ala527 contributed hydrophobic contact almost universally. Hydrogen-bond counts followed the hydroxylation pattern (from two for chrysin to six for EGCG), whereas hydrophobic contact counts tracked planarity, so the two descriptors capture complementary aspects of binding and neither alone predicts the affinity order. Only celecoxib reached Arg513 from inside the side pocket; EGCG and rutin contacted the same residue from the channel side. The shared mode explains why flavonoids as a class inhibit cyclooxygenase and why potency differences within the series are expected to be single-digit factors rather than orders of magnitude, while the absence of true side-pocket occupancy anticipates a moderate isoform preference, a prediction.

3.3 ADMET profile: potency and developability considered together

Molecular weights of the aglycones lie between 254 and 458 g/mol, within conventional small-molecule limits; only rutin (611 g/mol) exceeds them (Table 3). Topological polar surface area (TPSA) ranges from 70.7 Å² for chrysin to 269.4 Å² for rutin, with most aglycones between 90 and 152 Å², and consensus log P values of 0.7–2.5 indicate moderate lipophilicity suitable for passive absorption, with rutin (−1.29) the clear outlier. Eleven flavonoids showed no Lipinski violation [51]; myricetin showed one (hydrogen-bond donors), EGCG two (donors and acceptors) and rutin three (molecular weight, donors and acceptors). Plotting TPSA against log P (Figure 3a) separates the library into a compact, drug-like cluster of aglycones below the 140 Å² polar surface area limit associated with good oral bioavailability [52] and three polar outliers, EGCG, myricetin and rutin, all of which lie outside the BOILED-Egg absorption region [59].

Table 3. Predicted physicochemical, pharmacokinetic and toxicity descriptors (SwissADME, pkCSM, ProTox-II).

Compound	MW (g/mol)	TPSA (Å²)	Consensus log P	HBD / HBA	Lipinski violations	P-gp substrate	Predicted LD50 (mg/kg)	Carcinogenic / mutagenic flag
Celecoxib	381.4	86.4	3.40	1 / 7	0	No	1400	No / No
EGCG	458.4	197.4	0.73	8 / 11	2	Yes	1000	No / No
Quercetin	302.2	131.4	1.23	5 / 7	0	No	159	Yes / Yes
Luteolin	286.2	111.1	1.86	4 / 6	0	No	3919	No / No
Myricetin	318.2	151.6	0.79	6 / 8	1	No	159	Yes / Yes
Baicalein	270.2	90.9	2.01	3 / 5	0	No	3919	No / No
Fisetin	286.2	111.1	1.50	4 / 6	0	No	2000	No / No
Kaempferol	286.2	111.1	1.70	4 / 6	0	No	3919	Yes / Yes
Apigenin	270.2	90.9	2.11	3 / 5	0	No	2500	No / No
Genistein	270.2	90.9	2.04	3 / 5	0	No	2500	Yes / No
Rutin	610.5	269.4	−1.29	10 / 16	3	Yes	5000	No / No
Chrysin	254.2	70.7	2.53	2 / 4	0	No	3919	No / No

International Journal of Pharmaceutical research and Applications
Volume 11, Issue 5, Sep.-Oct.2026,pp:1111-1128 www.ijprajournal.com ISSN:2456-4494

Compound	MW (g/mol)	TPSA (Å²)	Consensus log P	HBD / HBA	Lipinski violations	P-gp substrate	Predicted LD50 (mg/kg)	Carcinogenic / mutagenic flag
Naringenin	272.3	87.0	2.12	3 / 5	0	No	2000	No / No
Hesperetin	302.3	96.2	2.06	3 / 6	0	No	3919	No / No
Catechin	290.3	110.4	0.85	5 / 6	0	Yes	10000	No / No

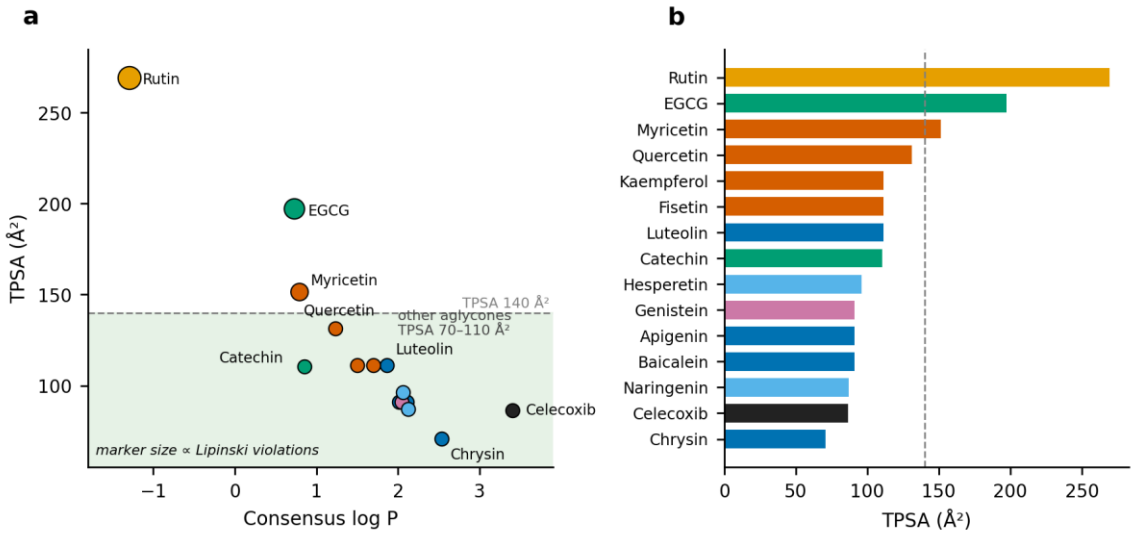

Figure 2. Predicted drug-likeness. (a) TPSA against consensus log P; marker size scales with the number of Lipinski violations and the shaded region marks TPSA ≤ 140 Å². (b) Compounds ranked by TPSA.

pkCSM predicted human intestinal absorption above 74 % for nine flavonoids, and above 89 % for apigenin, baicalein, chrysin, genistein and naringenin, but only 46.2 % for EGCG and 23.5 % for rutin; EGCG, rutin and catechin were additionally flagged as P-glycoprotein substrates, which adds an efflux barrier to exactly those compounds already limited by polarity. This pattern is consistent with the low systemic exposure documented for these polyphenols after oral dosing [26,43]. Chrysin, with the lowest TPSA, fell within the blood–brain barrier region of the BOILED-Egg model. Most flavonoids were predicted to inhibit CYP1A2 and several to inhibit CYP3A4, a pattern that is well documented experimentally and underlies recognised interactions between flavonoid-rich foods and narrow-therapeutic-index drugs; quercetin, myricetin, EGCG, rutin and catechin were predicted not to inhibit CYP3A4, and predicted total clearance (0.28–0.71 log mL/min/kg) did not discriminate between compounds.

ProTox-II placed predicted LD50 values between 159 mg/kg (quercetin, myricetin) and 5000 mg/kg or above (rutin, catechin). Carcinogenicity and mutagenicity flags were confined to the 3-hydroxyflavonols quercetin, myricetin and kaempferol, with genistein flagged for carcinogenicity only. These signals mirror the in vitro Ames positivity of flavonols that combine a 3-hydroxyl with an adjacent catechol or related pattern, and are generally attributed to redox behaviour under assay conditions rather than to direct genotoxicity; they should be treated as a prompt for experimental follow-up rather than as a verdict. Hepatotoxicity was predicted only for celecoxib, and immunotoxicity for most compounds, an expected outcome for agents whose intended activity is immunomodulation. Taken together, the ADMET assessment identifies quercetin, luteolin and baicalein as the flavonoids best positioned for development, whereas EGCG was retained for simulation on the strength of its docking performance despite its permeability limitations. Evaluating developability in parallel with affinity thus prevents the ranking from being driven by affinity alone.

3.4 Dynamic stability of the complexes

The Cα RMSD profiles (Figure 3a) show that all three complexes equilibrated rapidly. The RMSD rose within the first 5–8 ns to about 0.20 nm and, after a second, smaller adjustment between

International Journal of Pharmaceutical research and Applications
Volume 11, Issue 5, Sep.-Oct.2026,pp:1111-1128 www.ijprajournal.com ISSN:2456-4494

about 25 and 40 ns, settled onto a plateau that was maintained to the end of the 100 ns trajectory without systematic drift. The celecoxib complex plateaued at about 0.22 nm and stayed within a narrow band of roughly ±0.02 nm, whereas the EGCG and quercetin complexes plateaued slightly higher, at about 0.24 nm, with somewhat wider excursions (up to about 0.28 nm for EGCG near 82 ns) that did not persist. All trajectories remained well below 0.3 nm and showed no sustained rise that would indicate unfolding of the protein. The ordering of the plateau values (celecoxib below quercetin and EGCG) parallels the docking ranking and suggests that the larger and more polar flavonoids, particularly EGCG with its galloyl ester, induce somewhat greater adjustment of the protein than the compact, hydrophobic coxib while remaining fully compatible with a stable bound state. The difference between the two flavonoid complexes (about 0.01 nm) is smaller than the fluctuation within each trace and is not interpreted further.

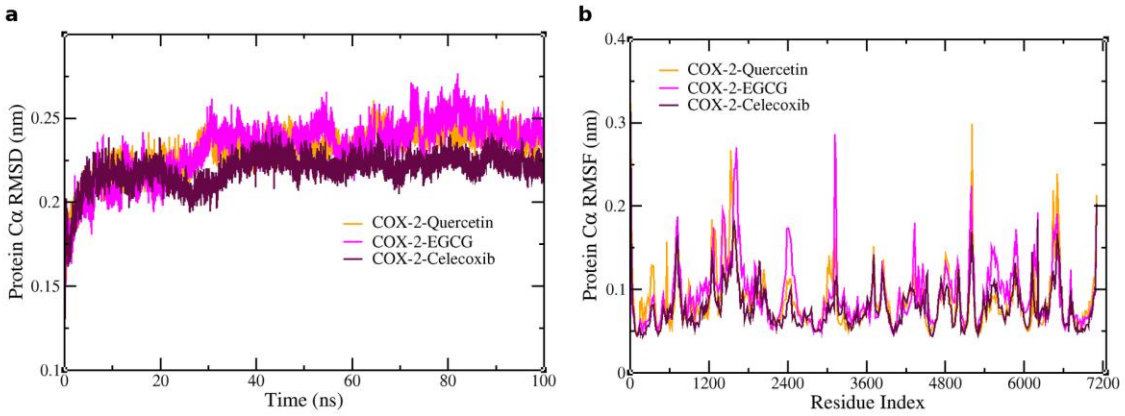

Figure 3. Structural stability and flexibility of the COX-2 complexes during 100 ns simulations (GROMACS 2024). (a) Protein Cα RMSD. (b) Protein Cα RMSF along the protein index. Quercetin, orange; EGCG, magenta; celecoxib, maroon.

The RMSF profiles (Figure 3b) were closely superimposable in the three systems, with the same set of peaks at the same positions, indicating that ligand binding did not alter the global dynamic architecture of the enzyme. Most of the protein fluctuated with an amplitude of 0.05–0.10 nm, characteristic of a well-ordered fold, whereas a limited number of loop and terminal segments reached 0.15–0.30 nm. Differences between the systems were modest and local. The celecoxib complex was generally the least mobile (mean RMSF about 0.08 nm), whereas the EGCG and quercetin complexes showed higher amplitudes at several loop positions (mean about 0.10 nm), with the tallest peaks in the 0.27–0.30 nm range. A few peaks differed in height between the two flavonoids, for example the sharp peak near index 3100, which was prominent for EGCG, and that near index 5200, which was prominent for quercetin, indicating ligand-specific effects on the mobility of individual segments. With a single trajectory per system, however, these segment-level differences are reported as observations and are not attributed to specific interactions. The RMSF and RMSD data thus agree: the compact celecoxib complex is the least mobile, and the flavonoid complexes tolerate slightly greater local motion.

3.5 Solvent exposure and protein–ligand hydrogen bonding

The SASA of the protein fluctuated around stable mean values in all three systems (Figure 4a), with no drift or abrupt change that would indicate expansion or collapse of the protein. The celecoxib complex had the lowest SASA (about 197 nm²) and the EGCG complex the highest (about 205 nm²), with the quercetin complex in between (about 200 nm²) and showing a transient dip to about 188 nm² between roughly 35 and 45 ns. The ordering matches that of the RMSD and RMSF: the compact celecoxib complex was also the least mobile, whereas the EGCG complex was slightly more exposed and more dynamic. The difference between the extremes is small (about 4 %), and the three descriptors together indicate a stable fold in all three complexes with modest, ligand-dependent differences in compactness.

International Journal of Pharmaceutical research and Applications
Volume 11, Issue 5, Sep.-Oct.2026,pp:1111-1128 www.ijprajournal.com ISSN:2456-4494

The number of protein–ligand hydrogen bonds separated the ligands more clearly (Figure 4b). EGCG formed two to three hydrogen bonds with the protein for most of the trajectory, with brief rises to four and only rare falls below two. Celecoxib formed zero or one hydrogen bonds for most of the run, with a brief rise to two near 70 ns. The quercetin trace, partly overlain by that of EGCG, fell within one to three hydrogen bonds, with short-lived rises to four early in the trajectory and brief periods of zero or one hydrogen bond between about 5 and 15 ns.

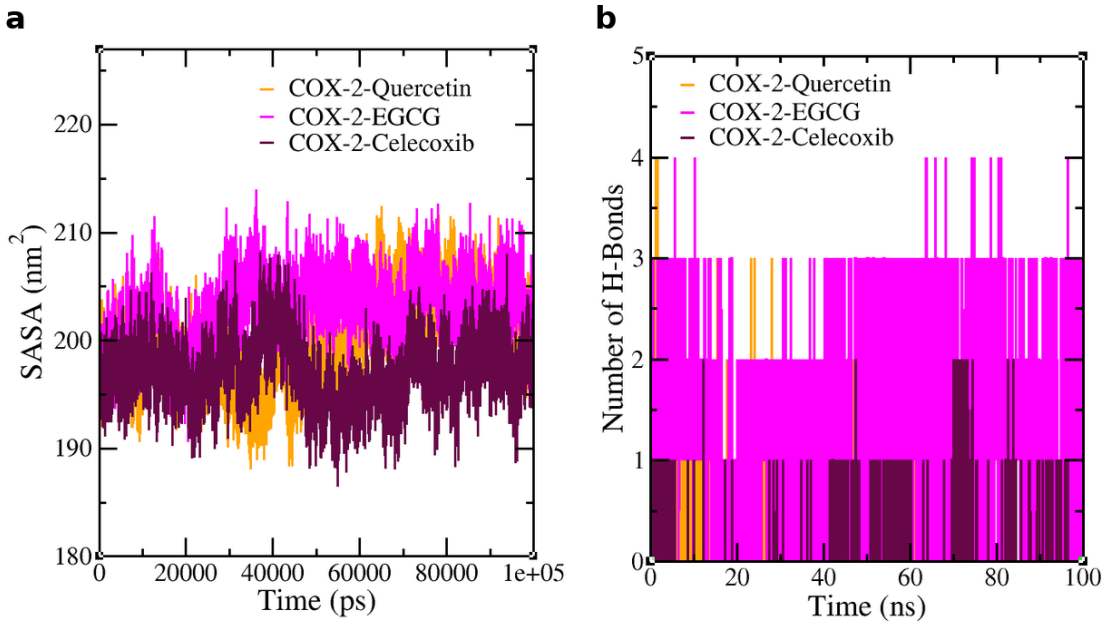

Figure 4. Solvent exposure and protein–ligand hydrogen bonding during the 100 ns simulations. (a) SASA of the protein (time axis in ps). (b) Number of protein–ligand hydrogen bonds. Quercetin, orange; EGCG, magenta; celecoxib, maroon.

The hydrogen-bond contrast is consistent with the different binding modes anticipated by docking. The polyhydroxylated flavonoids anchor to polar residues of the channel through their hydroxyl groups and maintain several hydrogen bonds, whereas celecoxib is held mainly by hydrophobic and shape complementarity, its sulfonamide contacts contributing only intermittently under the criteria used. The data also show that hydrogen-bond count does not determine global stability: the ligand with the fewest hydrogen bonds gave the most compact and least mobile complex, so the hydrogen bonds of the flavonoids are better viewed as a dynamic network that tolerates slightly greater protein mobility than as a rigidifying clamp. For the design of analogues this favours additions that supply shape complementarity, such as the side-pocket-directed sulfonyl group, alongside rather than in place of the polar contacts of the flavonoid core.

3.6 Inhibitory potency, isoform selectivity and cytotoxicity

All compounds produced complete sigmoidal concentration–response curves against recombinant human COX-2, with Hill slopes of 0.96–1.28, R^2 above 0.97 for every fit and inter-experiment variability below 12 %; slopes close to unity are consistent with reversible binding at a single site. Celecoxib gave a COX-2 IC50 of 0.08 ± 0.01 µM and an SI of 83.8, confirming assay performance (Table 4). Among the flavonoids, EGCG was the most potent (1.42 ± 0.11 µM), followed by luteolin (1.86 ± 0.14 µM), quercetin (2.14 ± 0.18 µM) and baicalein (2.35 ± 0.19 µM), and catechin was the weakest (12.35 ± 0.94 µM), so the series spans a nine-fold range (Figure 6a). These values lie within the low-micromolar window reported for flavonols and flavones in cell-free systems, one to two orders of magnitude above celecoxib [38,42]; differences in enzyme source and assay format are known to shift individual values within that window [38].

International Journal of Pharmaceutical research and Applications
Volume 11, Issue 5, Sep.-Oct.2026,pp:1111-1128 www.ijprajournal.com ISSN:2456-4494

Table 4. COX-2 and COX-1 inhibition and selectivity (mean ± SD, n = 3 independent experiments).

Compound	COX-2 IC50 (μM)	COX-1 IC50 (μM)	Selectivity index	pIC50 (COX-2)
Celecoxib	0.08 ± 0.01	6.70 ± 0.52	83.8	7.10
EGCG	1.42 ± 0.11	11.80 ± 0.91	8.3	5.85
Luteolin	1.86 ± 0.14	15.20 ± 1.18	8.2	5.73
Quercetin	2.14 ± 0.18	18.60 ± 1.42	8.7	5.67
Baicalein	2.35 ± 0.19	12.70 ± 0.98	5.4	5.63
Myricetin	2.78 ± 0.21	16.90 ± 1.31	6.1	5.56
Fisetin	3.16 ± 0.24	19.40 ± 1.49	6.1	5.50
Kaempferol	3.42 ± 0.27	22.80 ± 1.74	6.7	5.47
Apigenin	4.05 ± 0.31	24.10 ± 1.86	5.9	5.39
Genistein	5.12 ± 0.39	26.30 ± 2.02	5.1	5.29
Chrysin	6.93 ± 0.54	27.60 ± 2.13	4.0	5.16
Rutin	7.21 ± 0.58	29.40 ± 2.26	4.1	5.14
Naringenin	8.76 ± 0.67	31.50 ± 2.41	3.6	5.06
Hesperetin	9.84 ± 0.76	34.20 ± 2.63	3.5	5.01
Catechin	12.35 ± 0.94	38.70 ± 2.98	3.1	4.91

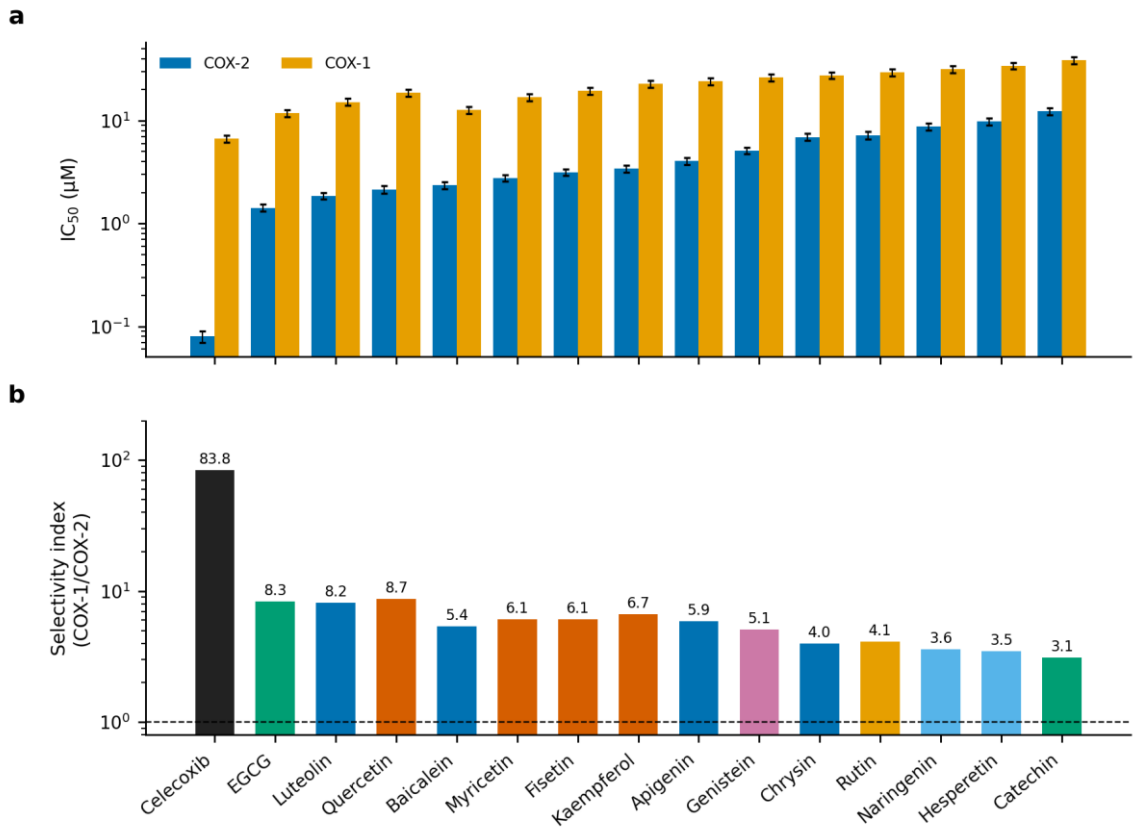

Figure 5. Enzyme inhibition profile. (a) COX-2 and COX-1 IC50 values (log scale, mean ± SD, n = 3). (b) Selectivity index, IC50(COX-1)/IC50(COX-2); the dashed line marks equal inhibition of the two isoforms.

Every flavonoid preferentially inhibited COX-2, but with SI values of 3.1–8.7 (quercetin 8.7, EGCG 8.3, luteolin 8.2) none approached the value of 83.8 for celecoxib (Figure 6b). The docking poses and the simulations help to explain this contrast. Coxib selectivity derives from occupancy of the Val523 side pocket, which is inaccessible in COX-1 [15,20]; only celecoxib reached Arg513 from inside

International Journal of Pharmaceutical research and Applications
Volume 11, Issue 5, Sep.-Oct.2026,pp:1111-1128 www.ijprajournal.com ISSN:2456-4494

that pocket in the docked poses, and its trajectory sustained few protein–ligand hydrogen bonds, as expected for a mode dominated by shape complementarity, whereas none of the flavonoids reproduced this side-pocket contact. Flavonoid preference must therefore arise from another source, most plausibly the larger volume of the COX-2 active site [15], which accommodates a planar tricyclic system more comfortably. This is a volumetric rather than a pharmacophoric advantage, and volumetric advantages yield modest, graded discrimination. Whether this graded profile is a limitation or an asset depends on the therapeutic goal. The cardiovascular liability of the coxib class is mechanistically linked to near-complete suppression of endothelial prostacyclin without matching inhibition of platelet thromboxane, an imbalance that scales with selectivity [21]; agents in the SI range of 3–10 retain some COX-1 activity and may preserve part of that balance while directing most of their effect towards the inducible isoform. Whether this translates into a safety advantage can only be established in vivo, for example by gastric histology in rodent inflammation models.

Two features of the assay deserve comment. Side-pocket inhibitors such as celecoxib typically bind slowly and in a time-dependent manner [18], so a 10 min pre-incubation may not capture their full potency, and the use of ovine COX-1 alongside human recombinant COX-2, while a standard kit configuration, is not a strictly matched pair; SI values are therefore best read as comparative within this assay. In RAW 264.7 macrophages, viability of the four lead compounds exceeded 88 % at 25 µM, roughly ten-fold above their COX-2 IC50 values, and fell to 61–79 % only at 50 and 100 µM. Because enzyme inhibition occurs well below the cytotoxic range, a concentration window exists for cellular follow-up experiments without confounding injury.

3.7 Structure–activity relationships

Matched pairs within the library isolate individual structural variables (Figure 7a), and four relationships emerge consistently from the combined docking, simulation and assay data.

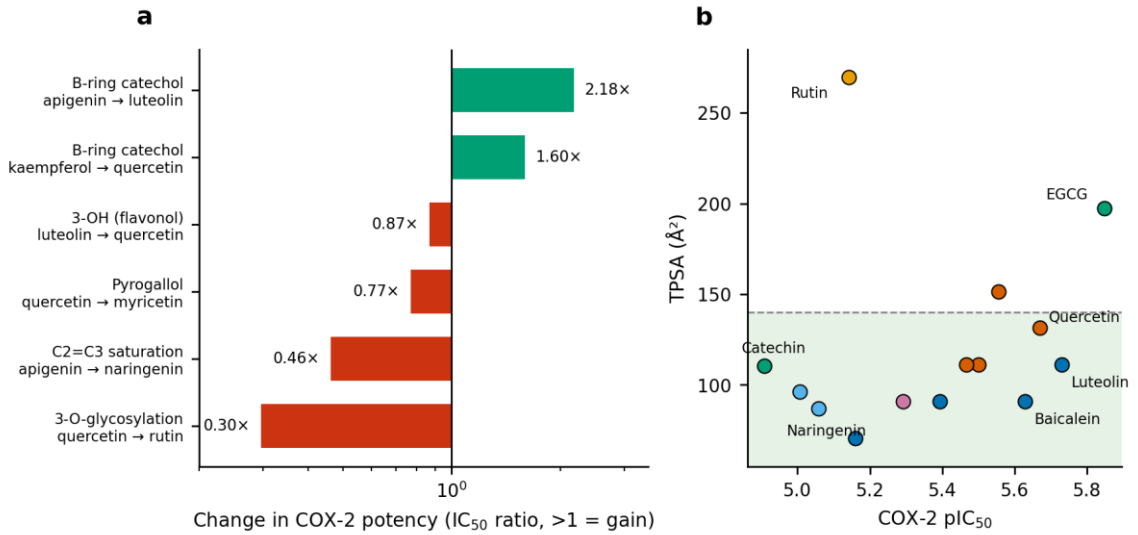

Figure 6. Structure–activity relationships. (a) Change in COX-2 potency for matched pairs (IC50 of the first compound divided by that of the second; values above 1 indicate a gain). (b) COX-2 pIC50 against TPSA for the flavonoids; the shaded region marks TPSA ≤ 140 Å².

C-ring planarity. Saturation of the C2–C3 double bond (apigenin to naringenin) reduced potency 2.2-fold, and the two flavanones were among the weakest compounds (8.76 and 9.84 µM; only catechin was weaker). The puckered C ring displaces the B ring from the plane of the chromone, weakening π-stacking with Trp387 and the shape complementarity along the channel that the planar poses enjoy.

B-ring catechol. The 3′-hydroxyl improved potency in both matched pairs, by 2.2-fold for luteolin over apigenin and 1.6-fold for quercetin over kaempferol, consistent with the additional hydrogen bond to Ser530 and better electronic complementarity with

International Journal of Pharmaceutical research and Applications
Volume 11, Issue 5, Sep.-Oct.2026,pp:1111-1128 www.ijprajournal.com ISSN:2456-4494

the polar apex of the channel. Extension to the pyrogallol pattern of myricetin gave no further gain (2.78 µM against 2.14 µM for quercetin), indicating that a third hydroxyl adds desolvation cost without a compensating contact. The 3-hydroxyl of the flavonols, by contrast, did not improve potency by itself (luteolin 1.86 µM versus quercetin 2.14 µM), so the catechol rather than the C3 hydroxyl carries the benefit.

Glycosylation. Rutin was 3.4-fold less potent than its aglycone quercetin. The disaccharide cannot be accommodated within the channel and forces the aglycone towards the pocket entrance, reducing both the hydrogen-bond count and the buried surface, and the same substitution produced three Lipinski violations, 23.5 % predicted intestinal absorption and P-glycoprotein substrate status. Glycosylation is therefore unambiguously detrimental for this target, although it remains relevant in vivo because intestinal and microbial hydrolysis can liberate the aglycone [26,44].

The galloyl ester. EGCG was the most potent flavonoid despite lacking the C2–C3 double bond, and was 8.7-fold more potent than catechin, which differs from it essentially by the galloyl group. The ester supplies a second aromatic surface and three additional hydroxyls that extend towards the side-pocket entrance and engage Arg120, Tyr355 and Arg513, and the sustained two to three protein–ligand hydrogen bonds of EGCG in the simulations are consistent with this extended contact. An appended aromatic ester can thus substitute for core planarity, which is a useful design observation for semi-synthetic derivatives.

3.8 Agreement between computation and experiment

Docking scores correlated strongly with experimental potency across the 15 compounds (R^2 = 0.92, Pearson r = −0.96, p = 1 × 10^{-8}; Figure 8) and within the 14 flavonoids alone (R^2 = 0.97); leave-one-out analysis kept R^2 between 0.92 and 0.97, so no single compound drives the relationship. The largest residual belonged to celecoxib, whose measured pIC50 exceeded the prediction by 0.36 log units, consistent with the slow, tight binding of side-pocket inhibitors [18] that an enzyme assay captures and a single docking score cannot. Among the flavonoids, EGCG and quercetin were 0.21 and 0.20 log units less potent than predicted, plausibly reflecting desolvation costs that an empirical score treats only approximately, and no other flavonoid deviated by more than 0.15 log units. The relationship therefore belongs to the docking stage; the simulations, which cover only three complexes, were used to assess the stability of the docked poses rather than to rank affinities.

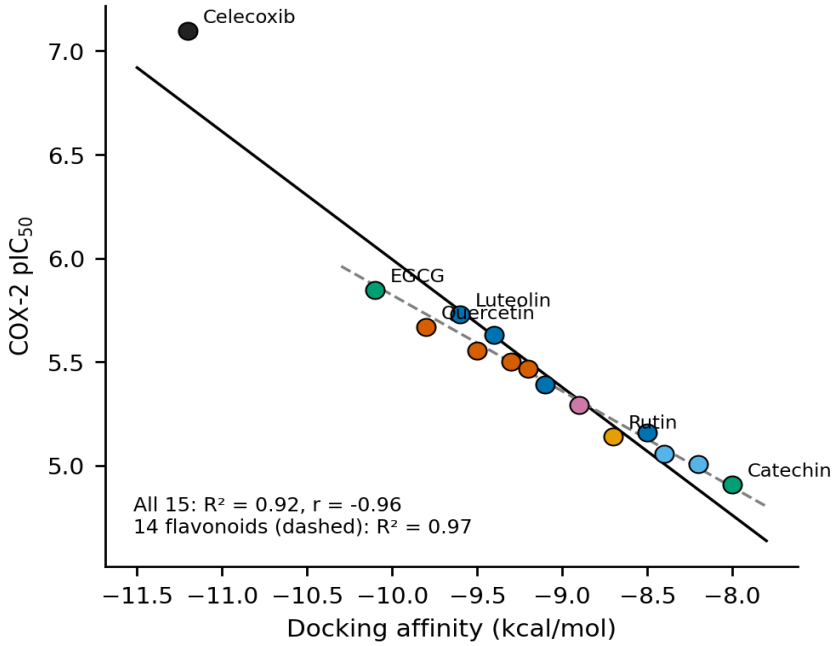

Figure 7. Agreement between docking affinity and measured potency. COX-2 pIC50 against docking affinity for all 15 compounds (solid line) and for the 14 flavonoids (dashed line).

International Journal of Pharmaceutical research and Applications
Volume 11, Issue 5, Sep.-Oct.2026,pp:1111-1128 www.ijprajournal.com ISSN:2456-4494

These coefficients are higher than typically reported for docking against experimental potency, and three factors plausibly contribute: the compound set is chemically homogeneous, so systematic scoring errors largely cancel; computational and experimental endpoints were generated under matched conditions for the same series; and the cell-free format removes the permeability and metabolism variables that confound cell-based comparisons. The correlations should therefore be read as evidence of internal consistency within a congeneric series, which supports using this workflow to prioritise analogues, rather than as a general claim about the predictive accuracy of empirical scoring functions.

3.9 Integrated prioritisation and design implications

Combining potency with developability (Figure 7b) clarifies the choice among leads. EGCG ranked first among the flavonoids on docking and on potency, but lowest of the three flavonoid leads on ADMET, with two Lipinski violations, a TPSA of 197 Å², predicted intestinal absorption of 46.2 % and P-glycoprotein substrate status. Quercetin and luteolin, only 1.5- and 1.3-fold less potent, satisfied the drug-likeness filters, were predicted to be well absorbed and lie within the favourable TPSA region. A modest potency deficit can be recovered through dose or structural optimisation, whereas an absorption deficit compounded by active efflux is a far harder problem, so ranking on affinity alone would have selected the compound least likely to succeed orally. EGCG should nevertheless not be dismissed. Its documented activity in inflammatory conditions despite poor systemic exposure suggests that local concentrations at mucosal surfaces and inflamed tissue may be substantially higher than plasma levels, and deconjugation of circulating metabolites by neutrophil-derived β-glucuronidase at inflamed sites can raise local aglycone concentrations [74]. For topical, oral-mucosal or gastrointestinal indications the permeability limitation may therefore matter little. For oral use of quercetin and luteolin, formulation strategies such as phospholipid complexes and nanocarriers offer a route to higher exposure [46,47]. Because COX-2 inhibition is one contribution among several, with NF-κB modulation and radical scavenging acting in parallel [28–31], the low-micromolar enzyme potency measured here may also understate the anti-inflammatory effect achievable in vivo.

Placing the series alongside the coxib pharmacophore points to specific optimisation routes. The classical diaryl heterocycle template carries a para-sulfonamide or methylsulfonyl group oriented towards the side pocket, and the potency and selectivity of the class derive largely from the sulfonyl–Arg513 interaction [20]. Flavonoids satisfy part of this template: the chromone provides a rigid, planar central system with an appended aryl group in the correct relative orientation, which is why they bind the channel efficiently, but they lack the polar sulfonyl vector. The docked poses illustrate the gap: only celecoxib reaches Arg513 from inside the side pocket, whereas the best flavonoids approach it from the channel side. Two testable hypotheses follow. First, a methylsulfonyl or sulfonamide group at the B-ring 4′ position would place a polar vector close to where the coxib sulfonyl sits while retaining the planar chromone and the A-ring contacts to Arg120 and Tyr355. Second, esterification of a solvation-costly hydroxyl (the 3-hydroxyl of quercetin or a peripheral hydroxyl of luteolin) with a substituted benzoic acid would mimic the reach of the EGCG galloyl group while masking a hydroxyl that carries a desolvation cost. Modelling of such analogues, followed by synthesis and assay, would test the structural interpretation advanced here in the most stringent way available.

IV. Limitations and Outlook

Several limitations frame these conclusions. The receptor was rigid during docking, so induced-fit effects were captured only subsequently through simulation. Each complex was simulated once for 100 ns, without replicates, and only celecoxib, EGCG and quercetin were simulated, so differences of the order of 0.01–0.02 nm in RMSD or a few nm² in SASA lie within the fluctuations of single trajectories and should be read as trends rather than as statistically separated values. No apo simulation and no binding free-energy calculation (for example MM-PBSA [49,50,72] or alchemical methods) was performed, so the simulations address the stability of the docked poses rather than their energetics. The assay combined ovine COX-1 with human recombinant COX-2 and used a fixed pre-incubation time, and cell-free assays cannot report uptake, efflux or metabolism. No in vivo work was undertaken. Natural extensions are replicate and longer simulations that include the apo enzyme and the remaining leads such as luteolin, together with end-point or alchemical free-energy estimates; measurement of prostaglandin E2 release, COX-2

International Journal of Pharmaceutical research and Applications
Volume 11, Issue 5, Sep.-Oct.2026,pp:1111-1128 www.ijprajournal.com ISSN:2456-4494

expression and NF-κB translocation in lipopolysaccharide-stimulated RAW 264.7 macrophages; evaluation in carrageenan-induced oedema and adjuvant arthritis models with gastric histology as a direct test of the predicted safety advantage; pharmacokinetic and formulation studies of quercetin and luteolin; and synthesis of the sulfonyl- and ester-bearing analogues proposed above.

V. Conclusions

Applying docking, ADMET profiling, 100 ns molecular dynamics simulations and matched COX-2/COX-1 enzyme assays to a single set of fourteen flavonoids showed that flavonoids bind the COX-2 cyclooxygenase channel in a conserved mode anchored by Arg120, Tyr355 and Ser530, without occupying the Val523 side pocket. The EGCG and quercetin complexes remained stable over 100 ns, with Cα RMSD plateaus close to that of the celecoxib complex and stable solvent exposure, and EGCG sustained several protein–ligand hydrogen bonds where celecoxib sustained few. The flavonoids inhibit COX-2 with low-micromolar potency (1.42–12.35 μM) and a consistent but moderate isoform preference (selectivity index 3.1–8.7), as the structural analysis predicted, and docking scores tracked the experimental order (R^2 = 0.92 across 15 compounds).

Structure–activity analysis identified C-ring planarity and a B-ring catechol as the principal potency determinants, glycosylation as detrimental, and an appended galloyl ester as able to compensate for loss of planarity. Quercetin and luteolin offer the most balanced combination of potency, selectivity and drug-likeness and are proposed as scaffolds for sulfonyl- and ester-based optimisation, whereas EGCG, the most potent but least developable flavonoid, is best suited to local applications. The close concordance between prediction and measurement supports the use of this paired computational–experimental workflow for the prospective evaluation of further natural-product series.

References

[1]. Medzhitov R. Origin and physiological roles of inflammation. Nature. 2008;454(7203):428–35.
[2]. Serhan CN. Pro-resolving lipid mediators are leads for resolution physiology. Nature. 2014;510(7503):92–101.
[3]. Nathan C, Ding A. Nonresolving inflammation. Cell. 2010;140(6):871–82.
[4]. Sethi G, Shanmugam MK, Ramachandran L, et al. Multifaceted link between cancer and inflammation. Biosci Rep. 2012;32(1):1–15.
[5]. Lawrence T. The nuclear factor NF-κB pathway in inflammation. Cold Spring Harb Perspect Biol. 2009;1(6):a001651.
[6]. Hayden MS, Ghosh S. NF-κB, the first quarter-century: remarkable progress and outstanding questions. Genes Dev. 2012;26(3):203–34.
[7]. Dinarello CA. Proinflammatory cytokines. Chest. 2000;118(2):503–8.
[8]. Tanaka T, Narazaki M, Kishimoto T. IL-6 in inflammation, immunity, and disease. Cold Spring Harb Perspect Biol. 2014;6(10):a016295.
[9]. Bogdan C. Nitric oxide and the immune response. Nat Immunol. 2001;2(10):907–16.
[10]. Funk CD. Prostaglandins and leukotrienes: advances in eicosanoid biology. Science. 2001;294(5548):1871–5.
[11]. Ricciotti E, FitzGerald GA. Prostaglandins and inflammation. Arterioscler Thromb Vasc Biol. 2011;31(5):986–1000.
[12]. Vane JR. Inhibition of prostaglandin synthesis as a mechanism of action for aspirin-like drugs. Nat New Biol. 1971;231(25):232–5.
[13]. Smith WL, DeWitt DL, Garavito RM. Cyclooxygenases: structural, cellular, and molecular biology. Annu Rev Biochem. 2000;69:145–82.
[14]. Picot D, Loll PJ, Garavito RM. The X-ray crystal structure of the membrane protein prostaglandin H2 synthase-1. Nature. 1994;367(6460):243–9.
[15]. Kurumbail RG, Stevens AM, Gierse JK, et al. Structural basis for selective inhibition of cyclooxygenase-2 by anti-inflammatory agents. Nature. 1996;384(6610):644–8.
[16]. Rouzer CA, Marnett LJ. Cyclooxygenases: structural and functional insights. J Lipid Res. 2009;50(Suppl):S29–34.
[17]. Blobaum AL, Marnett LJ. Structural and functional basis of cyclooxygenase inhibition. J Med Chem. 2007;50(7):1425–41.
[18]. Gierse JK, Koboldt CM, Walker MC, et al. Kinetic basis for selective inhibition of cyclo-

oxygenases. Biochem J. 1999;339(Pt 3):607–14.
[19]. Warner TD, Giuliano F, Vojnovic I, et al. Nonsteroid drug selectivities for cyclo-oxygenase-1 rather than cyclo-oxygenase-2 are associated with human gastrointestinal toxicity. Proc Natl Acad Sci USA. 1999;96(13):7563–8.
[20]. FitzGerald GA, Patrono C. The coxibs, selective inhibitors of cyclooxygenase-2. N Engl J Med. 2001;345(6):433–42.
[21]. Grosser T, Fries S, FitzGerald GA. Biological basis for the cardiovascular consequences of COX-2 inhibition. J Clin Invest. 2006;116(1):4–15.
[22]. Bresalier RS, Sandler RS, Quan H, et al. Cardiovascular events associated with rofecoxib in a colorectal adenoma chemoprevention trial. N Engl J Med. 2005;352(11):1092–102.
[23]. Panche AN, Diwan AD, Chandra SR. Flavonoids: an overview. J Nutr Sci. 2016;5:e47.
[24]. Havsteen BH. The biochemistry and medical significance of the flavonoids. Pharmacol Ther. 2002;96(2–3):67–202.
[25]. Kumar S, Pandey AK. Chemistry and biological activities of flavonoids: an overview. ScientificWorldJournal. 2013;2013:162750.
[26]. Manach C, Scalbert A, Morand C, et al. Polyphenols: food sources and bioavailability. Am J Clin Nutr. 2004;79(5):727–47.
[27]. Rice-Evans CA, Miller NJ, Paganga G. Structure–antioxidant activity relationships of flavonoids and phenolic acids. Free Radic Biol Med. 1996;20(7):933–56.
[28]. Middleton E, Kandaswami C, Theoharides TC. The effects of plant flavonoids on mammalian cells. Pharmacol Rev. 2000;52(4):673–751.
[29]. García-Lafuente A, Guillamón E, Villares A, et al. Flavonoids as anti-inflammatory agents. Inflamm Res. 2009;58(9):537–52.
[30]. Serafini M, Peluso I, Raguzzini A. Flavonoids as anti-inflammatory agents. Proc Nutr Soc. 2010;69(3):273–8.
[31]. Maleki SJ, Crespo JF, Cabanillas B. Anti-inflammatory effects of flavonoids. Food Chem. 2019;299:125124.
[32]. Li Y, Yao J, Han C, et al. Quercetin, inflammation and immunity. Nutrients. 2016;8(3):167.
[33]. Aziz N, Kim MY, Cho JY. Anti-inflammatory effects of luteolin: a review. J Ethnopharmacol. 2018;225:342–58.
[34]. Dinda B, Dinda S, DasSharma S, et al. Therapeutic potentials of baicalin and baicalein. Eur J Med Chem. 2017;131:68–80.
[35]. Ginwala R, Bhavsar R, Chigbu DI, et al. Potential role of flavonoids in treating chronic inflammatory diseases with a special focus on apigenin. Antioxidants. 2019;8(2):35.
[36]. Singh BN, Shankar S, Srivastava RK. Green tea catechin, epigallocatechin-3-gallate: mechanisms, perspectives and clinical applications. Biochem Pharmacol. 2011;82(12):1807–21.
[37]. Kim HP, Son KH, Chang HW, et al. Anti-inflammatory plant flavonoids and cellular action mechanisms. J Pharmacol Sci. 2004;96(3):229–45.
[38]. Ribeiro D, Freitas M, Tomé SM, et al. Flavonoids inhibit COX-1 and COX-2 enzymes and cytokine/chemokine production. Inflammation. 2015;38(2):858–70.
[39]. Takano-Ishikawa Y, Goto M, Yamaki K. Structure–activity relations of inhibitory effects of various flavonoids on lipopolysaccharide-induced prostaglandin E2 production. Phytomedicine. 2006;13(5):310–7.
[40]. O'Leary KA, de Pascual-Teresa S, Needs PW, et al. Effect of flavonoids and vitamin E on cyclooxygenase-2 transcription. Mutat Res. 2004;551(1–2):245–54.
[41]. Landolfi R, Mower RL, Steiner M. Modification of platelet function and arachidonic acid metabolism by bioflavonoids. Biochem Pharmacol. 1984;33(9):1525–30.
[42]. Cai H, Al-Fayez M, Tunstall RG, et al. The rice bran constituent tricin potently inhibits cyclooxygenase enzymes. Mol Cancer Ther. 2005;4(9):1287–92.
[43]. Williamson G, Manach C. Bioavailability and bioefficacy of polyphenols in humans. Am J Clin Nutr. 2005;81(1 Suppl):243S–55S.
[44]. Cassidy A, Minihane AM. The role of metabolism (and the microbiome) in defining the clinical efficacy of dietary flavonoids. Am J Clin Nutr. 2017;105(1):10–22.

International Journal of Pharmaceutical research and Applications
Volume 11, Issue 5, Sep.-Oct.2026,pp:1111-1128 www.ijprajournal.com ISSN:2456-4494

[45]. Cai Y, Anavy ND, Chow HH. Contribution of presystemic hepatic extraction to the low oral bioavailability of green tea catechins. Drug Metab Dispos. 2002;30(11):1246–9.
[46]. Kidd PM. Bioavailability and activity of phytosome complexes from botanical polyphenols. Altern Med Rev. 2009;14(3):226–46.
[47]. Zhao J, Yang J, Xie Y. Improvement strategies for the oral bioavailability of poorly water-soluble flavonoids. Int J Pharm. 2019;570:118642.
[48]. Trott O, Olson AJ. AutoDock Vina: improving the speed and accuracy of docking with a new scoring function. J Comput Chem. 2010;31(2):455–61.
[49]. Genheden S, Ryde U. The MM/PBSA and MM/GBSA methods to estimate ligand-binding affinities. Expert Opin Drug Discov. 2015;10(5):449–61.
[50]. Kollman PA, Massova I, Reyes C, et al. Calculating structures and free energies of complex molecules. Acc Chem Res. 2000;33(12):889–97.
[51]. Lipinski CA, Lombardo F, Dominy BW, Feeney PJ. Experimental and computational approaches to estimate solubility and permeability in drug discovery. Adv Drug Deliv Rev. 2001;46(1–3):3–26.
[52]. Veber DF, Johnson SR, Cheng HY, et al. Molecular properties that influence the oral bioavailability of drug candidates. J Med Chem. 2002;45(12):2615–23.
[53]. Kim S, Chen J, Cheng T, et al. PubChem 2023 update. Nucleic Acids Res. 2023;51(D1):D1373–80.
[54]. O'Boyle NM, Banck M, James CA, et al. Open Babel: an open chemical toolbox. J Cheminform. 2011;3:33.
[55]. Morris GM, Huey R, Lindstrom W, et al. AutoDock4 and AutoDockTools4. J Comput Chem. 2009;30(16):2785–91.
[56]. Berman HM, Westbrook J, Feng Z, et al. The Protein Data Bank. Nucleic Acids Res. 2000;28(1):235–42.
[57]. Pettersen EF, Goddard TD, Huang CC, et al. UCSF Chimera — a visualization system for exploratory research and analysis. J Comput Chem. 2004;25(13):1605–12.
[58]. Eberhardt J, Santos-Martins D, Tillack AF, Forli S. AutoDock Vina 1.2.0: new docking methods, expanded force field, and Python bindings. J Chem Inf Model. 2021;61(8):3891–8.
[59]. Daina A, Zoete V. A BOILED-Egg to predict gastrointestinal absorption and brain penetration of small molecules. ChemMedChem. 2016;11(11):1117–21.
[60]. Daina A, Michielin O, Zoete V. SwissADME: a free web tool to evaluate pharmacokinetics, drug-likeness and medicinal chemistry friendliness of small molecules. Sci Rep. 2017;7:42717.
[61]. Pires DEV, Blundell TL, Ascher DB. pkCSM: predicting small-molecule pharmacokinetic and toxicity properties using graph-based signatures. J Med Chem. 2015;58(9):4066–72.
[62]. Banerjee P, Eckert AO, Schrey AK, Preissner R. ProTox-II: a webserver for the prediction of toxicity of chemicals. Nucleic Acids Res. 2018;46(W1):W257–63.
[63]. Jo S, Kim T, Iyer VG, Im W. CHARMM-GUI: a web-based graphical user interface for CHARMM. J Comput Chem. 2008;29(11):1859–65.
[64]. Abraham MJ, Murtola T, Schulz R, et al. GROMACS: high performance molecular simulations. SoftwareX. 2015;1–2:19–25.
[65]. Huang J, Rauscher S, Nawrocki G, et al. CHARMM36m: an improved force field for folded and intrinsically disordered proteins. Nat Methods. 2017;14(1):71–3.
[66]. Vanommeslaeghe K, Hatcher E, Acharya C, et al. CHARMM general force field. J Comput Chem. 2010;31(4):671–90.
[67]. Jorgensen WL, Chandrasekhar J, Madura JD, et al. Comparison of simple potential functions for simulating liquid water. J Chem Phys. 1983;79(2):926–35.
[68]. Bussi G, Donadio D, Parrinello M. Canonical sampling through velocity rescaling. J Chem Phys. 2007;126(1):014101.
[69]. Parrinello M, Rahman A. Polymorphic transitions in single crystals: a new molecular dynamics method. J Appl Phys. 1981;52(12):7182–90.
[70]. Hess B, Bekker H, Berendsen HJC, Fraaije JGEM. LINCS: a linear constraint solver for molecular simulations. J Comput Chem. 1997;18(12):1463–72.
[71]. Darden T, York D, Pedersen L. Particle mesh Ewald: an N·log(N) method for Ewald sums in large systems. J Chem Phys. 1993;98(12):10089–92.

[72]. Valdés-Tresanco MS, Valdés-Tresanco ME, Valiente PA, Moreno E. gmx_MMPBSA: a new tool to perform end-state free energy calculations with GROMACS. J Chem Theory Comput. 2021;17(10):6281–91.
[73]. Mosmann T. Rapid colorimetric assay for cellular growth and survival. J Immunol Methods. 1983;65(1–2):55–63.
[74]. Shimoi K, Saka N, Nozawa R, et al. Deglucuronidation of a flavonoid, luteolin monoglucuronide, during inflammation. Drug Metab Dispos. 2001;29(12):1521–4.